JAM CM Journal of Applied Mathematics and Computational Mechanics 2024, 23(4), 133-144
www.amcm.pcz.pl p-ISSN 2299-9965
DOI: 10.17512/jamcm.2024.4.12 e-ISSN 2353-0588

NUMERICAL SIMULATION OF OXYGEN DISTRIBUTION IN SOFT TISSUE EXPOSED TO AN EXTERNAL HEAT IMPULSE

Maria Zadoń, Marek Jasiński

Department of Computational Mechanics and Engineering, Silesian University of Technology
Gliwice, Poland
maria.zadon@polsl.pl, marek.jasinski@polsl.pl

Received: 24 July 2024; Accepted: 10 December 2024

Abstract. The purpose of this study is to analyse the effect of elevated temperature on oxygen distribution in biological tissue. The effect of temperature and thermal tissue damage on the values of thermophysical parameters was considered. Changes in the perfusion coefficient affect blood velocity in the capillary, thereby influencing the distribution of partial oxygen pressure. In the tissue area, the effect of myoglobin was taken into account. Furthermore, the effect of mitochondrial clustering on oxygen distribution was also analysed. The finite difference method and the shooting method were used in the numerical implementation stage.

MSC 2010: *65M06, 80A20, 80A30, 92C10*
Keywords: *bioheat transfer, oxygen transport, myoglobin saturation, mitochondrial clustering, finite difference method, shooting method*

1. Introduction

One of the most important functions of blood is to carry oxygen from the lungs to the tissues. Gas exchange between blood and tissue takes place in the smallest blood vessels, the capillaries. Elevated temperature, caused by factors such as external heat, can alter the properties of tissues and, in some cases, even cause thermal damage, disrupting the vasculature [1, 2] and oxygen delivery [3]. Factors that can delay the onset of hypoxia or lack of oxygen in the body include myoglobin and the phenomenon of mitochondrial clustering.

Myoglobin (Mb) is a protein responsible for oxygen transport and local oxygen storage. Through a dense network of capillaries, oxygen is transferred from hemoglobin to tissue, where oxidative phosphorylation occurs, resulting in the production of energy in the form of ATP in the mitochondria. Additionally, myoglobin improves oxygen diffusion in areas with low partial oxygen pressure, which improves tissue resistance to hypoxia, contributing to the maintenance of oxygen homeostasis [4-6]. Mitochondria, on the other hand, have the ability to move and relocate within the cell, thus also influencing the regulation of various cellular processes. In cases

of oxygen deficiency, they tend to accumulate near the capillaries, where oxygen access is facilitated [3, 7].

Mathematical models of the oxygen distribution are often based on the Krogh cylinder theory. A model takes into account the capillary and surrounding cylindrical area of the tissue. The equations for both subdomains are included in this model, with partial oxygen pressure used as the main variable [5, 8]. Furthermore, the Krogh model can incorporate equations related to, for example, hemoglobin saturation in the capillary subdomain and myoglobin saturation in the tissue subdomain [4-6]. Although the author of this model initially adopted numerous simplifications, his work has become the foundation for many subsequent studies, including on various therapies, the presence of cancers, and angiogenesis processes in the body [3-5]. For an extensive discussion of various aspects of the theory of oxygen transport to tissue, including issues related to the Krogh cylinder model, see [4].

The temperature field in biological tissue is modeled using one of the selected bioheat transfer equations: Pennes, Cattaneo-Vernotte or dual-phase lag (DPL) equations in which additional components of internal heat sources related to perfusion and metabolism are considered [3, 9-13]. In addition, the variation of the thermophysical parameters of the tissue depending on temperature and/or thermal damage is taken into account, the latter being most often evaluated on the basis of the so-called Arrhenius scheme [1, 2, 14].

The work concerns the analysis of the effect of elevated temperature on the distribution of oxygen in biological tissue. The bioheat transfer model was used, represented by a 3D area of homogeneous tissue and an oxygen distribution model in the form of an axisymmetric Krogh cylinder model, the latter using the values of the variable perfusion coefficient calculated in the bioheat transfer task. On the basis of this coefficient, the blood velocity in the capillary, which is one of the parameters of the oxygen distribution model, is calculated. Models for combined analysis of bioheat and oxygen distribution are rare in the literature; moreover, to the best of the authors' knowledge, a model that takes into account the effect of myoglobin on oxygen distribution in the tissue during heating has not been considered to date. In addition, the presented model takes into account the phenomenon of mitochondria clustering through a new proposed function in which the oxygen demand depends on the level of oxygen partial pressure at a given section of the capillary.

2. Governing equations

In this work, a model in the form of a cubic biological tissue, on which an external heat flux operates, and an axisymmetric model of the so-called Krogh cylinder were used to analyze oxygen distribution (Fig. 1 (left)). The latter corresponds to a capillary, surrounded by tissue, in which oxygen from the blood reaches the tissue area. Note that capillary sizes are of the order of micrometers (in this work $R_c = 2.5$ μm, $R_t = 25$ μm, $L_t = 500$ μm), while the domain dimensions for thermal analysis are $1.5 \times 1.5 \times 1.5$ cm. For this reason, the entire structure of the blood vessel

is not considered, but a single Krogh cylinder, placed at a selected point located in the bioheat task domain is taken into account.

Thermal analysis is based on the bioheat transport equation in the Pennes formulation with adequate boundary initial conditions [3, 10]

$$\begin{aligned}
&\mathbf{x}\in\Omega: \quad c\dot{T}=\nabla\left[\lambda(T)\nabla T\right]+Q_{met}+Q_{perf}, \quad Q_{perf}=c_B\,w(T_B-T)\\
&\mathbf{x}\in\Gamma_0: \quad q_0=\begin{cases} q_{0,max}\exp\left(-\dfrac{2(x^2+y^2)}{r_{imp}^2}\right), & \text{for } t\le t_{exp}\\ 0, & \text{for } t>t_{exp}\end{cases}\\
&\mathbf{x}\in\Gamma_c: \quad q(\mathbf{x},t)=0\\
&t=0: \quad T(\mathbf{x},t)=T_{init}
\end{aligned} \tag{1}$$

where λ [W m^{-1} K^{-1}] is the thermal conductivity of tissue, c [J m^{-3} K^{-1}] is the volumetric specific heat, Q_{perf} [W m^{-3}] and Q_{met} [W m^{-3}] are heat sources related to perfusion and metabolism, respectively, w [(m$^3_{blood}$/s)/(m$^3_{tissue}$)] is the perfusion coefficient, c_B [J m^{-3} K^{-1}] is the volumetric specific heat of the blood, and T_B is the arterial blood temperature. T stands for temperature, while $\dot{T}$ is its time derivative, $q_{0,max}$ [W m^{-2}] denotes the maximal value of the heat flux, r_{imp} is the radius of the impulse, t_{exp} [s] is the exposure time, T_{init} denotes the initial tissue temperature. The boundary Γ_0 is the outer surface of the tissue domain on which the heat flux q_0 is applied, while Γ_c is the remaining part of the boundary.

Due to the increase in tissue temperature, its thermophysical parameters may change. In this study, the thermal conductivity varies with temperature (in Kelvin) [1], and the tissue volumetric specific heat of the tissue is related to the thermal conductivity [15] according to the functions presented in the article [14]. Tissue exposed to an external heat impulse can be thermally damaged. Using the Arrhenius scheme, the degree of thermal damage to the tissue is estimated based on the formula [2, 10]

$$Arr(\mathbf{x},t^F)=\int_0^{t^F} A\exp\left[-\frac{E}{RT(\mathbf{x},t)}\right]\mathrm{d}t \tag{2}$$

where A [s^{-1}] is the preexponential factor, E [J mol^{-1}] is the activation energy, and R [J mol^{-1} K^{-1}] is the universal gas constant. The integral values of $Arr = 1$ and $Arr = 4.6$ are used as a threshold for tissue necrosis, corresponding to a probability of 63 % and 99 % of cell death at a given point **x**.

According to the literature [2], the perfusion coefficient is defined as a function that represents the phenomena that occur in the tissue as the temperature increases

$$w=w(Arr)=w_0\sum_{i=0}^{2} m_i Arr^i \tag{3}$$

where w_0 [s^{-1}] is the initial blood perfusion coefficient and m_i are the polynomial coefficients. The coefficient values are assumed to be $m_0 = 1$, $m_1 = 25$, $m_2 = -260$ for $Arr = [0,0.1]$ (the initial increase in the perfusion due to vasodilation), $m_0 = 1$, $m_1 = -1$, $m_2 = 0$ for $Arr = (0.1,1]$ (the stage of decrease in blood flow resulting from the vasculature shut down), while for $Arr > 1$ $m_0 = m_1 = m_2 = 0$.

The value of the perfusion coefficient calculated on the base (3) is then used to calculate blood velocity in the capillary u_b [cm s^{-1}], a parameter found in the oxygen distribution model. As already mentioned, the dimensions of the two models used are at different scales (cm vs. μm), so the entire capillary network is not considered but only a single Krogh cylinder. Therefore, the relationship between the thermal damage-dependent perfusion coefficient $w(Arr)$ and the blood velocity in the capillary is the link between the two models used. It is in the form of [3, 16]

$$u_b = w(Arr) L_t \frac{R_t^2}{R_c^2} \tag{4}$$

Figure 1 (right) illustrates the relationship between the oxygen partial pressure and the saturation of myoglobin (Mb) and hemoglobin (Hb). Knowledge of these relationships is essential in the oxygen distribution model, and the level of saturation of hemoglobin S_{Hb} and myoglobin S_{Mb} is calculated as follows [4, 5, 8, 16]

$$S_{Hb}(P_b) = \frac{P_b^n}{P_b^n + P_{50}^n}, \quad S_{Mb}(P_t) = \frac{P_t}{P_t + P_{50,Mb}} \tag{5}$$

where P_{50} [mmHg] is the half-maximal hemoglobin saturation, n is the Hill coefficient, $P_{50,Mb}$ [mmHg] is the half-maximal myoglobin saturation. The following parameters were assumed for the dissociation curves shown in Figure 1 (right): $n = 2.57$, $P_{50} = 27$ mmHg, $P_{50,Mb} = 5$ mmHg.

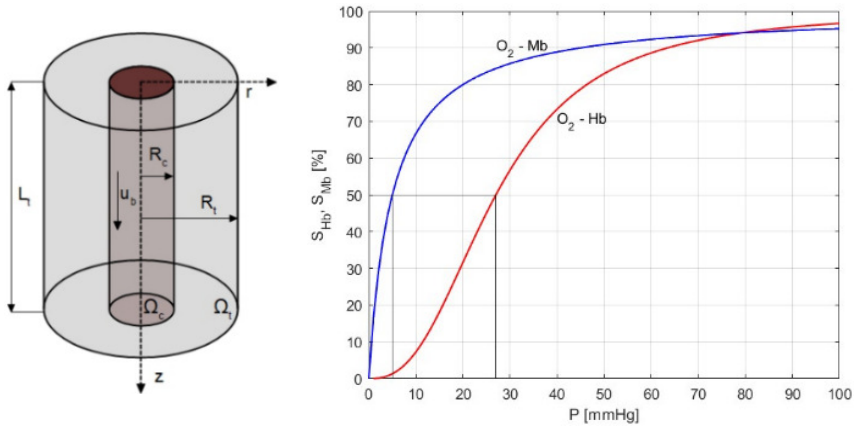

Fig. 1. Axisymmetric Krogh cylinder model, oxyhemoglobin, and myoglobin-O_2 dissociation curves

In this work, two separate equations for the radial and axial directions for the oxygen distribution model have been considered. The following governing equations with boundary conditions were used to describe the radial distribution of oxygen in the tissue subdomain [5, 6, 14]

$$\begin{aligned} &r \in \Omega_t: \ \frac{1}{r}\frac{d}{dr}\left[rK_t \frac{dP_t(r)}{dr} + rc_{Mb} D_{Mb} \frac{d\left[S_{Mb}(P_t)\right]}{dr} \right] = M_t(P_t), \ \ M_t(P_t) = \frac{M_0 P_t(r)}{P_{crit} + P_t(r)} \\ &r = R_c: \ 2\pi R_c K_t \frac{dP_t(r)}{dr} = -k\left(P_b - P_t(r)\right) \\ &r = R_t: \ \frac{dP_t(r)}{dr} = 0 \end{aligned} \tag{6}$$

where P_t [mmHg] is the partial pressure of oxygen in the tissue, K_t [(cm^2 s^{-1})(mol cm^{-3} mmHg^{-1})] is the Krogh diffusion coefficient, c_{Mb} [mol cm^{-3}] is the tissue concentration of myoglobin, D_{Mb} [cm^2 s^{-1}] is the diffusion coefficient in the tissue, M_0 [mol cm^{-3} s^{-1}] is the oxygen demand, P_{crit} [mmHg] is the half--maximum oxygen consumption, P_b [mmHg] is a partial pressure of oxygen in the blood, k [(cm^2 s^{-1})(mol cm^{-3} mmHg^{-1})] is the mass transfer coefficient.

It should be noted that this type of model has not yet been used in analysis related to the presence of oxygen in the tissue. While the main assumptions of the basic equation to account for the influence of myoglobin come from [6], the oxygen consumption model $M_t(P_t)$ in the form of Michaelis-Menten kinetics was introduced, and a boundary condition at the capillary-tissue interface was adopted, assuming instances of intravascular resistance during oxygen diffusion into the tissue area [16]. Both elements make it possible to more accurately reflect the processes occurring during the phenomenon under study.

For the axial direction, oxygen partial pressure in the blood is given by [16]

$$\begin{aligned} &z \in \Omega_c: \ \ \pi R_c^2 u_b \kappa_b \frac{d\left[S_{Hb}(P_b)\right]}{dz} = -k\left[P_b - P_t(R_c)\right] \\ &z = 0: \ \ \ P_b = P_{b\,inlet} \end{aligned} \tag{7}$$

where Q_b [cm^3 s^{-1}] is the blood flow rate in the capillary and κ_b [mol cm$^{-3}{}_{blood}$] is the oxygen carrying capacity of the blood.

In summary, in the first step of analysis, the bioheat transfer task is solved, the temperature values (Eq. (1)), the Arrhenius integral (Eq. (2)) and the perfusion coefficient (Eq. (3)) are calculated, then, for a selected point of the bioheat problem domain and selected time steps, the oxygen distribution is estimated on the basis of equations (5)-(7), with the blood velocity in the capillary calculated using (4).

3. Methods of solution

In the numerical implementation stage, the explicit scheme of the finite-difference method was used to solve the bioheat transfer problem, while the shooting method was applied to solve the task of determining the distribution of oxygen partial pressure in the Krogh cylinder model. Figure 2 on the left shows the differential grid with nodes where the results of solving the bioheat transfer equation were obtained. For the considered transient thermal analysis model in 3D, a 7 – point stencil was used (Fig. 2 (right)).

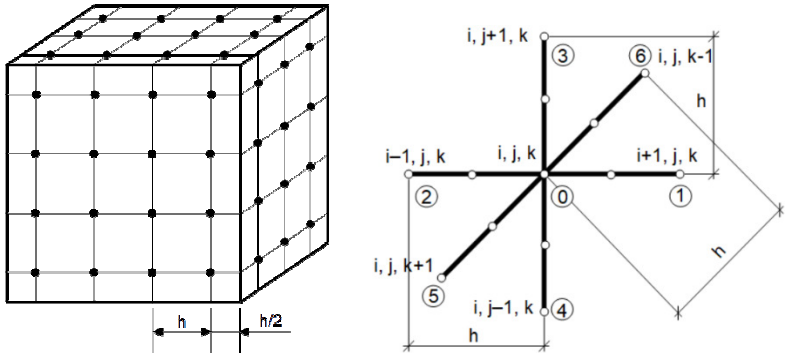

Fig. 2. Differential grid and the 7-point stencil used in the bioheat transfer problem

Taking into account the differential quotients presented in the paper [14], the equation for the central node of the stencil can be written in its final form:

$$T_0^f = T_0^{f-1} + \frac{\Delta t}{ch}\sum_{e=1}^{6}\lambda_{0e}\left(T_e^{f-1} - T_0^{f-1}\right) + \frac{c_B w \Delta t}{c}\left(T_B - T_0^{f-1}\right) + \frac{\Delta t}{c}Q_{met} \tag{8}$$

To solve the model related to the oxygen distribution in the radial direction, the shooting method was used. The idea of this method is to transform a boundary value problem (BVP) into an initial value problem (IVP). At first, the boundary condition at the selected boundary, denoted Γ_{shoot}, is used as the initial condition for the IVP. However, the second initial condition must be guessed. In the next step, the value of the obtained IVP solution is compared with the known boundary condition at the opposite boundary Γ_{target}. The procedure is repeated iteratively until the results agree. To estimate the guess value, approximate methods are used to solve equations, and the initial problem is solved using algorithms for solving ordinary differential equations. This paper uses the Newton method and the 4th-order Runge-Kutta method and assumes $r = R_c$ as Γ_{target} [17].

The Newton method for solving nonlinear equations requires the definition of guess values in consecutive iterations.

$$\alpha^{i+1} = \alpha^i - \frac{\phi(\alpha^i)}{\phi'(\alpha^i)}, \quad i \geq 0 \tag{9}$$

Then, the solution of two IVPs is found, one resulting from the BVP transformation (equations (6) with (5)) and an additional one resulting from the use of the Newton method.

$$K_t P_t'' + K_t \frac{P_t'}{r} + c_{Mb} D_{Mb} \left[\frac{1}{r} \frac{P_{50,Mb} P_t'}{\left(P_t + P_{50,Mb}\right)^2} + \frac{P_{50,Mb} P_t''}{\left(P_t + P_{50,Mb}\right)^2} - \frac{2P_{50,Mb} (P_t')^2}{\left(P_t + P_{50,Mb}\right)^3} \right] = Q_V$$

$$P_t'(R_t) = 0 \qquad (10)$$

$$P_t(R_t) = \alpha$$

$$K_t Z'' + K_t \frac{Z'}{r} + c_{Mb} D_{Mb} \left[\frac{1}{r} \frac{P_{50,Mb} Z'}{\left(Z + P_{50,Mb}\right)^2} + \frac{P_{50,Mb} Z''}{\left(Z + P_{50,Mb}\right)^2} - \frac{2P_{50,Mb} (Z')^2}{\left(Z + P_{50,Mb}\right)^3} \right] = Q_V'$$

$$Z'(R_t) = 0 \qquad (11)$$

$$Z(R_t) = 1$$

$$Z = \frac{\partial P_t(R_c, \alpha)}{\partial \alpha}, \quad Z' = \frac{\partial P_t'(R_c, \alpha)}{\partial \alpha}, \quad Q_V' = \frac{\partial Q_V}{\partial \alpha}, \quad Q_V = M_t(P_t) \qquad (12)$$

After finding the solution of IVP, the following differences are checked:

$$\begin{aligned} \phi(R_c, \alpha) &= P_t'(R_c, \alpha) + e_1 P_t(R_c, \alpha) - e_2, \quad & e_1 &= -k/(2\pi R_c K_t) \\ \phi'(R_c, \alpha) &= Z'(R_c, \alpha) + e_1 Z(R_c, \alpha), & e_2 &= e_1 P_b \end{aligned} \qquad (13)$$

After determination of the partial pressure in tissue P_t in the radial direction for a given node m, the saturation S_{Hb} is calculated in the next node $m+1$ on the basis of (cf. equation (7))

$$S_{Hb,m+1} = -\frac{kh_z}{Q_b \kappa_b} \left(P_{b,m} - P_{t,m} \right) + S_{Hb,m}, \quad m = 0,1,...,nz \qquad (14)$$

where nz is the number of nodes in the axial direction. Next, the partial pressure in the capillary P_b in the node $m+1$ is also determined using the equation (5).

4. Results of computations

In the study, a biological tissue domain in the shape of a cube $15 \times 15 \times 15$ mm was analysed. To reduce computation time, only a quarter of the area was considered, and the number of nodes $76 \times 76 \times 151$ needed for discretisation using the finite

difference method. The following thermophysical parameters were used for heat transfer calculations: $c_B = 3.9962$ MJ m^{-3} K^{-1}, $w_0 = 0.041$ s^{-1}, $Q_{met} = 245$ W m^{-3}, $T_B = 37$ °C, while for boundary-initial condition: $q_{0,max} = 18\,000$ W m^{-2}, $t_{exp} = 22$ s, $T_{init} = 37$ °C. The thermal damage model assumes the following values: $A = 3.1 \cdot 10^{98}$ s^{-1}, $E = 6.27 \cdot 10^5$ J mol^{-1}, $R = 8.314$ J mol^{-1} K^{-1} [3, 18].

The following data were used in the calculations for the oxygen distribution model: $R_c = 2.5$ µm, $R_t = 25$ µm, $L_t = 500$ µm, $K_t = 1.9845 \cdot 10^{-14}$ (cm^2 s^{-1})(mol cm^{-3} mmHg^{-1}), $P_{crit} = 1$ mmHg, $M_0 = 5 \cdot 10^{-8}$ mol cm^{-3} s^{-1}, $k = 2.79 \cdot 10^{-13}$ (cm^2 s^{-1})(mol cm^{-3} mmHg^{-1}), $P_{b\,inlet} = 100$ mmHg, $\kappa_b = 8.9286 \cdot 10^{-6}$ mol cm$^{-3}{}_{blood}$, $n = 2.57$, $P_{50} = 27$ mmHg [3, 5, 6, 16]. For the analysis of the impact of myoglobin, the following data related to oxygen transfer were used: $c_{Mb} = 5 \cdot 10^{-7}$ mol cm^{-3}, $D_{Mb} = 0.7 \cdot 10^{-6}$ cm^2 s^{-1}, $P_{50,Mb} = 5$ mmHg [4, 6]. When analysing the effect of mitochondrial clustering, the parameters associated with myoglobin (c_{Mb}, D_{Mb}, $P_{50,Mb}$) were assumed to be equal to zero in equation (6).

Figure 3 (left) shows the temperature distribution in the cube-shaped domain of tissue under consideration for 22 s, while Figure 3 (right) presents temperature courses at five selected control points within the same domain. Subsequently, the courses of the Arrhenius integral (Fig. 4 (left)) and the perfusion coefficient (Fig. 4 (right)) were determined. The coordinates of the control points are [cm]: A (0, 0, 0.273), B (0, 0, 0.462), C (0, 0, 0.482), D (0, 0, 0.502), E (0, 0, 0.651).

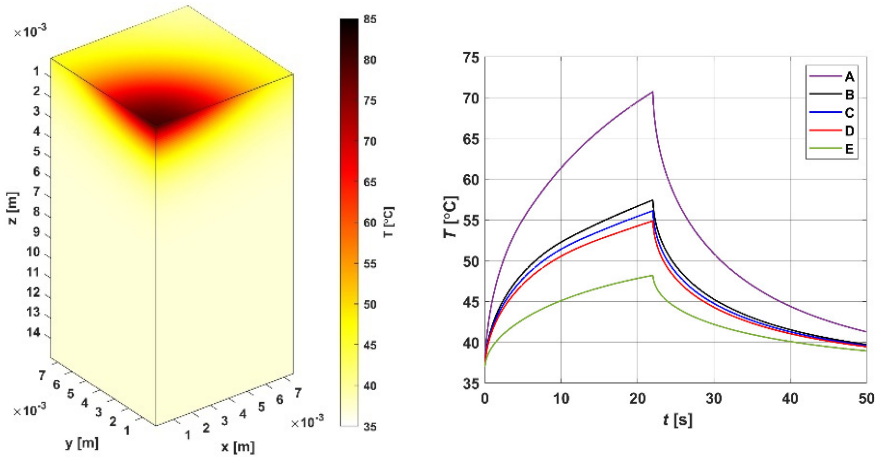

Fig. 3. Temperature distribution in the tissue for $t = 22$ s and temperature courses at selected nodes

As the temperature increases, there is a simultaneous increase in perfusion, resulting from the phenomenon of vasodilation. However, further elevation of the temperature leads to progressive thermal damage, ultimately resulting in the disappearance of perfusion. For the further calculations, point B was chosen to consider the Krogh cylinder, i.e. the oxygen distribution. For this point, the blood velocity in the capillary was calculated based on the course of the perfusion coefficient.

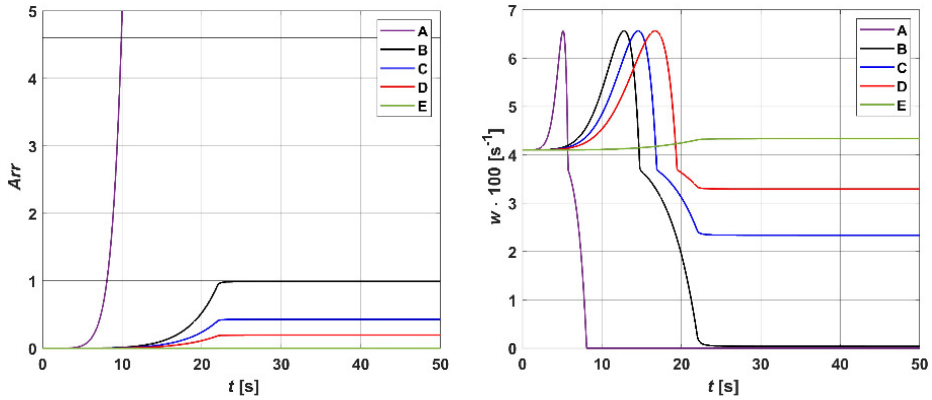

Fig. 4. Arrhenius integral and perfusion coefficient courses in selected nodes

For the analysis of the influence of mitochondria clustering on oxygen distribution, a new function is proposed. The tissue subdomain is divided into two regions: the one adjacent to the capillary ($R_c \le r \le (R_t - R_c)/2$), and the remaining region ($(R_t - R_c)/2 < r \le R_t$). Additionally, a threshold of 40 mmHg was assumed, as levels below this may result in tissue hypoxia. When $P_t(R_c) \ge 40$ mmHg, a constant value of M_0 is assumed for both regions, while for $P_t(R_c) < 40$ mmHg, an oxygen demand value is equal to $M_0 \cdot (1 + r/R_t)$ in the adjacent region, and $M_0 \cdot (1 - r/R_t)$ in the remaining region. Figure 5 shows a comparison of the results for two variants of the calculation, for $M_0 = \text{const}$, and the calculation with a function for the clustering of mitochondria. For the radial direction, the first curve is for the capillary inlet ($z = 0$), while the others are for $z = L_t/2$. The curves in the axial direction show the oxygen pressure in the capillary, indicating the onset of hypoxia after 22 s for both cases, with the difference that the mitochondrial clustering phenomenon caused a significant delay, and hypoxia occurred at $z = 0.035$ cm.

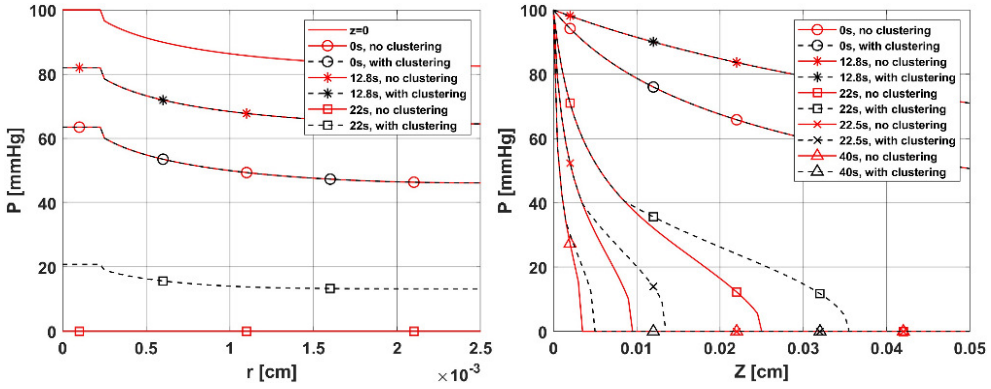

Fig. 5. Partial pressure of the oxygen distribution in the radial and axial directions for the case with and without mitochondrial clustering

The analysis also took into account the effect of myoglobin. Figure 6 shows the distributions of oxygen partial pressure in the radial and axial directions, with the distinction between the results obtained with and without consideration of myoglobin ($c_{Mb} = 0$, $D_{Mb} = 0$, $P_{50,Mb} = 0$). The distributions obtained confirm that myoglobin causes a slight delay in the appearance of hypoxia ($t = 22$ s).

The results of the oxygen distribution were compared with those reported in [6] and [16] (Fig. 7). For the results presented in [6], a comparison was made between the results for cases with and without myoglobin, noting that the oxygen consumption model in [6] was assumed to be zero-order kinetics, which, compared to the Michaelis-Menten kinetics used in the current work, always results in a much greater decrease in level of partial oxygen partial pressure in the radial direction in the tissue subdomain [4, 16]. Moreover, in [6], on the capillary-tissue interface, continuity of pressure was assumed, while in the current model the condition taking into account intravascular resistance was considered, which must mean lower $P_t(R_c)$ for the current model. Therefore, it can be concluded that the differences found in this case are justified, and the location of our results relative to the results of [6] is correct.

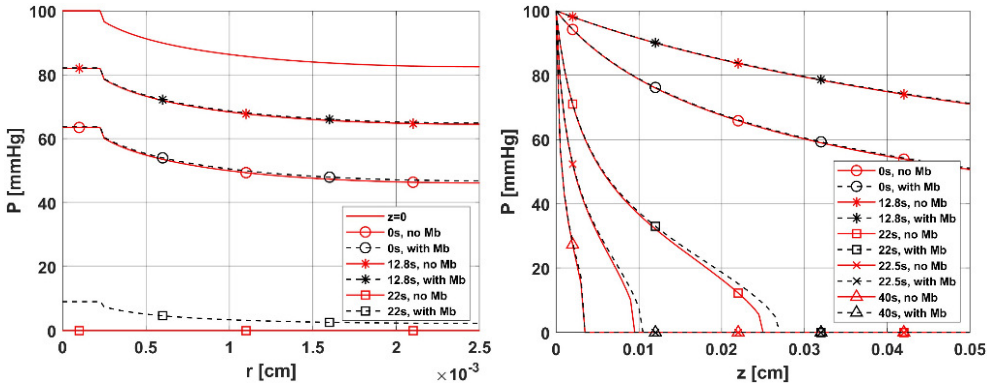

Fig. 6. Partial pressure of the oxygen distribution in radial and axial directions for the case with and without myoglobin

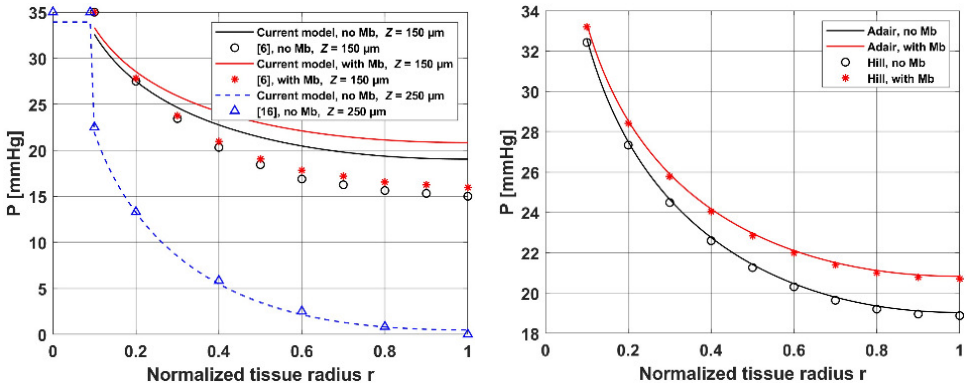

Fig. 7. Comparison of the results of the current model with the results in [6] and [16] and the results obtained for the current model using Hill and Adair ODCs

The model of [16] included intravascular resistance and a slightly different variant of mitochondria clustering. The results from the current model agree well with the results of this work; only the value of the P_b value is slightly lower by less than 2 mmHg.

In addition, Figure 7 (right) compares the results obtained from our model using different oxyhemoglobin dissociation curves. While the current model used Hill ODC, the results obtained using Adair ODC (also used in [6]) give very similar results, so it can be concluded that the choice of ODC did not matter much in the case studied. We have previously given a broader discussion and comparison of models with different ODCs in [14].

5. Conclusions

The results of the calculations indicate significantly that an external heat impulse influences the distribution of oxygen in tissue. Despite the cessation of impulse exposure after 22 s, the heat wave migrated toward the interior of the tissue (Figs. 3 (right) and 4), causing an increase in the value of tissue damage and changes in the perfusion coefficient w according to equation (3). Consequently, this affects blood velocity in the capillary u_b, a parameter that integrates models of bioheat transfer and oxygen distribution (Eq. (4)).

The two main findings of the current work refer to the oxygen distribution model:

– the clustering of mitochondria effectively delays the onset of hypoxia (Fig. 5),
– by including the effect of myoglobin in equation (6), hypoxia, resulting from a low blood velocity, occurs with a delay (Fig. 6).

Since oxygen consumption occurs primarily in mitochondria, clustering leads to a higher oxygen demand in areas with densely arranged mitochondria and lower demand where they are sparse [16]. Clusters of mitochondria are represented in the model as increased oxygen demand according to the authors' new function presented in Section 4. Previously, rather step functions were used [3, 16].

The major effect of myoglobin is observed after 22 s (Fig. 6), indicating that this protein only releases stored oxygen when there is an oxygen deficiency in the tissue. From the results presented, it can be concluded that incorporation of myoglobin-facilitated diffusion has relatively little effect on overall oxygen transport. These results are consistent with studies by Jurgens et al. [19] suggest that myoglobin is of minimal importance in oxygen transport under physiological conditions. Roy and Popel also reached similar conclusions [20].

References

[1] Oden, J.T., Diller, K.R., Bajaj, C., Browne, J.C., Hazle, J., Babuška, I., Bass, J., Biduat, L., Demkowicz, L., Elliott, A., Feng, Y., Fuentes, D., Prudhomme, S., Rylander, M.N., Stafford, R.J., & Zhang, Y. (2007). Dynamic data-driven finite element models for laser treatment of cancer. *Numerical Methods for Partial Differential Equations*, *23*(4), 904-922. DOI: 10.1002/NUM.20251.

[2] Abraham, J.P., & Sparrow, E.M. (2007). A thermal-ablation bioheat model including liquid--to-vapor phase change, pressure- and necrosis-dependent perfusion, and moisture-dependent

properties. *International Journal of Heat and Mass Transfer*, *50*(13-14), 2537-2544. DOI: 10.1016/J.IJHEATMASSTRANSFER.2006.11.045.

[3] Jasiński, M. (2022). Numerical analysis of thermal damage and oxygen distribution in laser irradiated tissue. *Journal of Applied Mathematics and Computational Mechanics*, *21*(2), 51-62. DOI: 10.17512/JAMCM.2022.2.05.

[4] Goldman, D. (2008). Theoretical models of microvascular oxygen transport to tissue. *Microcirculation*, *15*(8), 795-811. DOI: 10.1080/10739680801938289.

[5] Whiteley, J.P., Gavaghan, D.J., & Hahn, C.E.W. (2002). Mathematical modelling of oxygen transport to tissue. *Journal of Mathematical Biology*, *44*, 503-522. DOI: 10.1007/S002850200135.

[6] Fletcher, J.E. (1980). On facilitated oxygen diffusion in muscle tissues. *Biophysical Journal*, *29*(3), 437. DOI: 10.1016/S0006-3495(80)85145-9.

[7] Kurz, F.T., Aon, M.A., O'Rourke, B., & Armoundas, A.A. (2017). Functional implications of cardiac mitochondria clustering. *Advances in Experimental Medicine and Biology*, *982*, 1-24. DOI: 10.1007/978-3-319-55330-6_1.

[8] Zhu, T.C., Liu, B., & Penjweini, R. (2015). Study of tissue oxygen supply rate in a macroscopic photodynamic therapy singlet oxygen model. *Journal of Biomedical Optics*, *20*(3), 038001. DOI: 10.1117/1.JBO.20.3.038001.

[9] El-Nabulsi, R.A., & Anukool, W. (2022). Nonlocal thermal effects on biological tissues and tumors. *Thermal Science and Engineering Progress*, *34*, 101424. DOI: 10.1016/J.TSEP.2022.101424.

[10] Paruch, M. (2020). Mathematical modeling of breast tumor destruction using fast heating during radiofrequency ablation. *Materials (Basel, Switzerland)*, *13*(136), 455-458. DOI: 10.3390/MA 13010136.

[11] El-Nabulsi, R.A. (2021). Fractal Pennes and Cattaneo-Vernotte bioheat equations from product-like fractal geometry and their implications on cells in the presence of tumour growth. *Journal of the Royal Society Interface*, *18*(182), 20210564. DOI: 10.1098/RSIF.2021.0564.

[12] Majchrzak, E., & Stryczyński, M. (2021). Dual-phase lag model of heat transfer between blood vessel and biological tissue. *Mathematical Biosciences and Engineering: MBE*, *18*(2), 1573-1589. DOI: 10.3934/MBE.2021081.

[13] Alzahrani, F., & Abbas, I. (2022). A numerical solution of nonlinear DPL bioheat model in biological tissue due to laser irradiations. *Indian Journal of Physics*, *96*(2), 377-383. DOI: 10.1007/s12648-020-01988-w.

[14] Jasiński, M., & Zadoń, M. (2023). Modeling of the influence of elevated temperature on oxygen distribution in soft tissue. *Engineering Transactions*, *71*(3), 287-306. DOI: 10.24423/ENGTRANS .3086.20230426.

[15] Hamilton, G. (1998). *Investigations of the thermal properties of human and animal tissues, Ph.D. Thesis*. https://eleanor.lib.gla.ac.uk/record=b1789586.

[16] McGuire, B.J., & Secomb, T.W. (2001). A theoretical model for oxygen transport in skeletal muscle under conditions of high oxygen demand. *Journal of Applied Physiology*, *91*(5), 2255-2265. DOI: 10.1152/jappl.2001.91.5.2255.

[17] Keskin, A.Ü. (2019). Boundary Value Problems for Engineers. In: *Boundary Value Problems for Engineers*. Springer International Publishing. DOI: 10.1007/978-3-030-21080-9.

[18] Majchrzak, E., Turchan, L., & Jasiński, M. (2019). Identification of laser intensity assuring the destruction of target region of biological tissue using the gradient method and generalized dual--phase lag equation. *Iranian Journal of Science and Technology – Transactions of Mechanical Engineering*, *43*, 539-548. DOI: 10.1007/s40997-018-0225-2.

[19] Jürgens, K.D., Papadopoulos, S., Peters, T., & Gros, G. (2000). Myoglobin: Just an oxygen store or also an oxygen transporter? *News in Physiological Sciences*, *15*(5), 269-274. DOI: 10.1152/physiologyonline.2000.15.5.269.

[20] Roy, T.K., & Popel, A.S. (1996). Theoretical predictions of end-capillary PO2 in muscles of athletic and nonathletic animals at VO2max. *The American Journal of Physiology*, *271*(2 Pt 2). DOI: 10.1152/AJPHEART.1996.271.2.H721.